



Research paper

Synthesis, characterization and UV–visible study of schiff base-acetylene functionalized organosilatrane receptor for the dual detection of Zn²⁺ and Co²⁺ ions

Gurjaspreet Singh^{a,*}, Sushma^a, Priyanka^a, Suman^a, Diksha^a, Jashan Deep Kaur^a, Anamika Saini^a, Anita Devi^a, Pinky Satija^b

^a Department of Chemistry, Panjab University, Chandigarh 160014, India

^b School of Advanced Chemical Sciences, Shoolini University, Solan, Himachal Pradesh 173212, India



ARTICLE INFO

Keywords:

Schiff-base
Organosilatrane
Acetylene
UV–visible study
Zn²⁺ and Co²⁺ ions

ABSTRACT

The present article describes the synthesis of Schiff base-acetylene functionalized organosilatrane (**6a–6e**) and their characterization by ¹H and ¹³C NMR spectroscopy and ESI-QTOF mass spectrometry. The UV–visible study of the organosilatrane **6a** unveiled their high selectivity towards the recognition of Zn²⁺ and Co²⁺ ions without exhibiting any significant interference from other competitive metal ions. The calculated value of association constant with **6a** for Zn²⁺ and Co²⁺ ions was 0.11 × 10⁶ M⁻¹ and 0.24 × 10⁶ M⁻¹ and the limit of detection was 0.28 × 10⁻⁶ M and 0.82 × 10⁻⁶ M respectively. Furthermore, DFT calculations were performed to get an insight into the interacting behaviour of sensor **6a** towards Zn²⁺ and Co²⁺ ions.

1. Introduction

In recent years, the development of chemosensors for the identification of metal ions attains great attention in the research field because metal ions performs significant roles in the functioning of living organisms and plants [1]. They have been extensively used in energy storage devices, pharmaceuticals, paper, water, textiles and food industries [2]. However, the altered level of these metal ions is extremely harmful to human health and the environment [3].

Among various metal ions, Zn²⁺ and Co²⁺ ions are necessary vital elements for human beings. In humans, Zn²⁺ is the second most abundant transition metal ion and it helps in several physiological processes such as gene transcription, protein sequencing and regulation of metalloenzymes [4,5]. The surplus of Zn²⁺ ions causes several neurodegenerative diseases like Alzheimer's, Parkinson's, epilepsy, hypoxia–ischemia, arteriosclerosis and damage the pancreas while its deficiency causes stomach cramps, diabetes, skin diseases and infantile diarrhea [6,7]. It also performs important physiological functions in plants as it is the major component of different cofactors that regulate the enzyme activity [8,9]. The Zn²⁺ metal ions are widely employed in the industry in the protection process of steel and iron and for the manufacturing of batteries [10,11]. On the other hand, the Co²⁺ metal

ion is one of the essential metal ion in animals, plants, soils and rocks. It is the major component of vitamin B12 that helps in the iron metabolism, DNA synthesis, support formation of myelin and RBCs (Red Blood Cells) [12,13]. The excess of Co²⁺ ions in the body causes several health issues like cardiomyopathy, cardiac failure, asthma, thyroid damage and diminished pulmonary function while its deficiency causes pernicious anemia [14]. Apart from their biological importance, it is also used to accelerate the O₂/H₂ production in electrodes, sulphate-radical induced destruction of contaminants and improve the electrochromic properties of tungsten oxide nanowires [15–17]. So, the detection of Zn²⁺ and Co²⁺ ions is necessary in every field. A number of methods (atomic absorption/emission spectroscopy, electrochemical methods and inductively coupled plasma) have been used for their detection

but optical methods are preferred over these sophisticated instrumentation techniques because of their simplicity, excellent selectivity and high detection accuracy [18].

Organosilatrane is trigonal bipyramidal silicon molecules having three five-membered rings and a transannular dative bond between nitrogen and a silicon atom. Generally, they are represented as. Nowadays, they are attaining great attention because of their peculiar stereo-electronic and molecular structure which is responsible for their unique behaviour [19]. They have been popularly used in the field of sensing,

* Corresponding author at: Department of Chemistry and Centre of Advanced Studies, Panjab University, Chandigarh 160014, India.

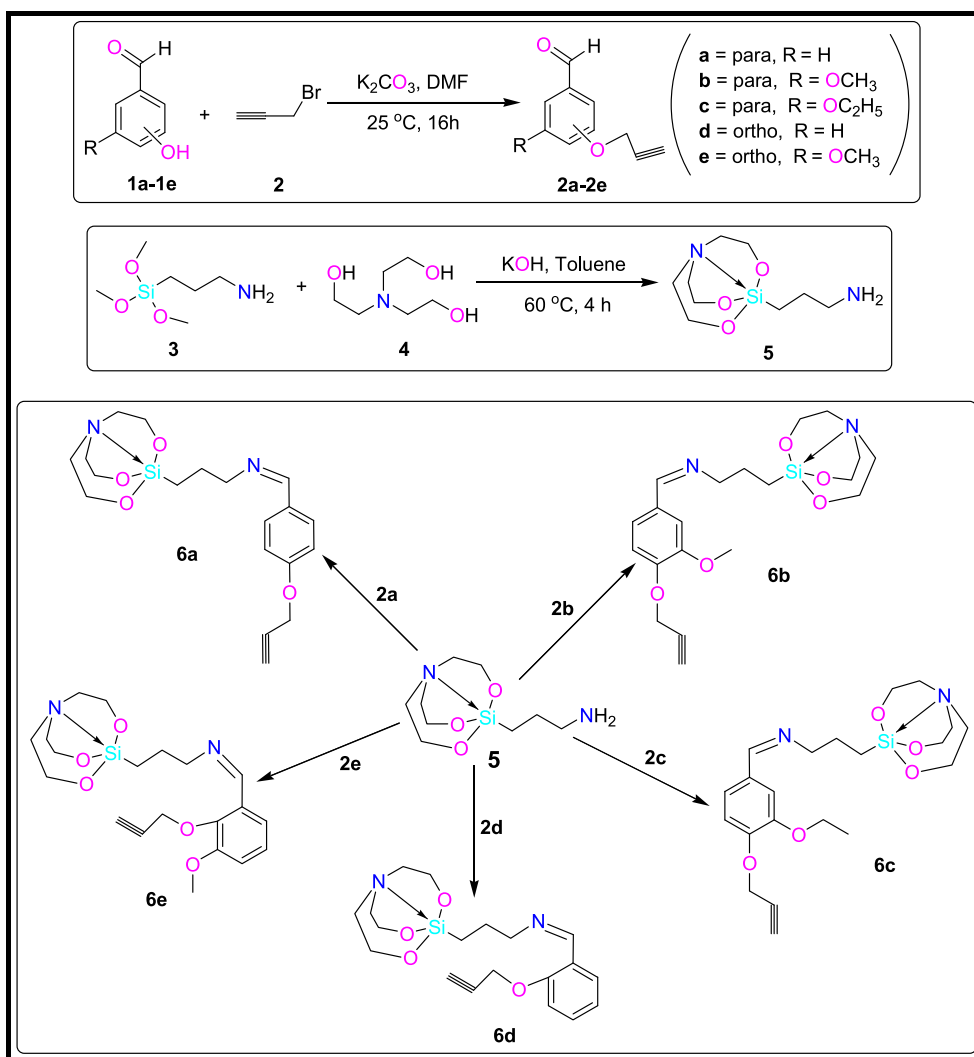
E-mail address: gjsingh@pu.ac.in (G. Singh).

<https://doi.org/10.1016/j.ica.2021.120465>

Received 23 April 2021; Received in revised form 18 May 2021; Accepted 18 May 2021

Available online 20 May 2021

0020-1693/© 2021 Elsevier B.V. All rights reserved.



Scheme 1. Schematic representation and reaction condition for the synthesis of Schiff base-acetylene functionalized organosilatrane (6a–6e): toluene, 60 °C, 6 h reflux.

nanoscience, biology and coating purposes [20–23]. Schiff base are represented by $R_1R_2C = NR'(R' \neq H)$ and show their widespread applications in various fields like nanoscience, biology, sensing, agriculture and material chemistry [24–27]. Further, the Schiff base linked acetylene moiety enhances their sensing capability and biological utility [28,29].

With an aspiration, we have synthesized the organosilatrane that contain biologically and materially important Schiff base and acetylene moiety into a single framework. The photophysical properties of the organosilatrane **6a** were examined by employing UV–visible spectroscopy towards the identification of Zn^{2+} and Co^{2+} ions over other metal ions.

2. Experimental section

2.1. Material and equipments

Propargyl bromide (80% in toluene) (Avra), substituted Hydroxybenzaldehyde (ortho and para) (Avra), Potassium carbonate (Avra), Potassium hydroxide (Avra), Aminopropyltrimethoxysilane (Aldrich),

Triethanolamine (Aldrich), dry toluene (Merck) and N, N'-dimethylformamide (DMF) (Merck) were used as received. Inorganic chloride salts of sodium, cobalt, barium, nickel, zinc, magnesium, silver, potassium, rubidium, cadmium, calcium, aluminium and cesium were bought from S.D. fine Chem. Ltd., India. Acetylene functionalized benzaldehyde and γ -aminopropylorganosilatrane was synthesized by known procedures from literature [30,20]. The Schlenk line was used to create N_2 atmosphere for addition purposes. The 1H (400 MHz) and ^{13}C (126 MHz) NMR spectra were recorded on the BRUKER AVANCE II spectrophotometer using $CDCl_3$ as an internal reference, and chemical shifts (δ) were reported relative to tetramethylsilane. The coupling constant (J) values are reported in Hz. The following abbreviations are used in NMR: s = singlet, d = doublet, t = triplet, q = quartet, p = pentet, m = multiplet. Mass spectral measurements were recorded with XEVO-G2-XS QTOF mass spectrometer. The UV–visible spectral measurements were carried out on the JASCO V-530 UV–visible spectrophotometer.

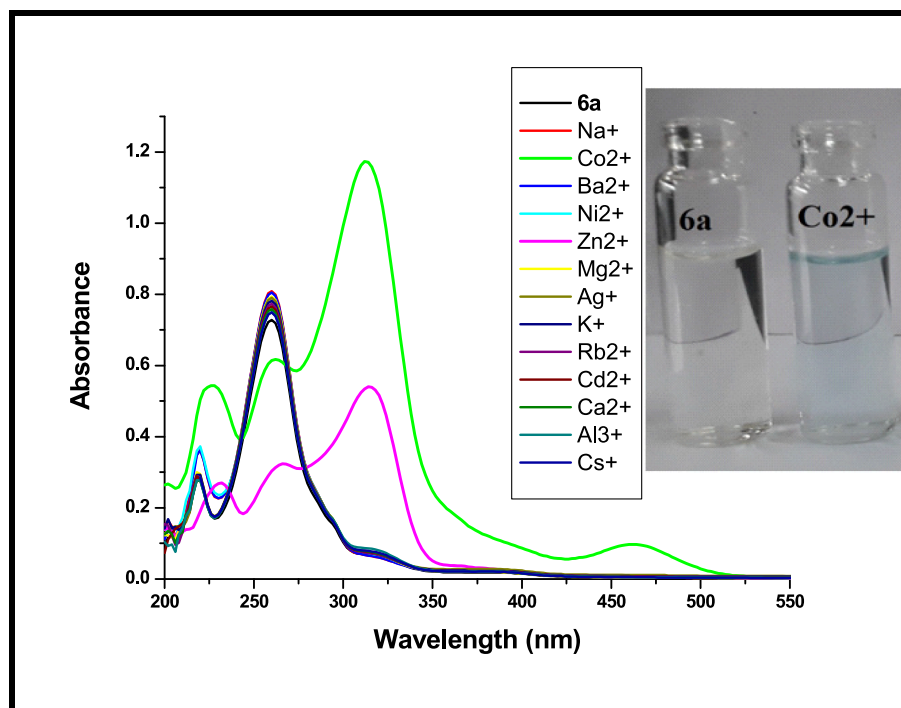


Fig. 1. UV-visible spectra of compound 6a in the presence of different metal ions in acetonitrile solution.

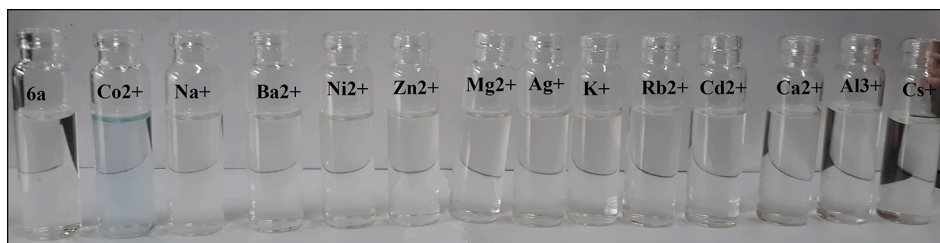


Fig. 2. The picture of compound 6a upon addition of different metal ions in acetonitrile solution.

2.2. Synthesis and characterization

2.2.1. General procedure for the synthesis of Schiff base-acetylene functionalized organosilatanes (6a–6e)

To a flame-dried 50 mL two-neck round bottom flask, the acetylene benzaldehyde (**2a–2e**) (1 equiv) and γ -aminopropylorganosilatrane (1 equiv) were added into 20 mL toluene under a dry N_2 atmosphere. Then the reaction mixture was refluxed for 6 h at 60 °C. After refluxing, the solvent was removed under reduced pressure using a vacuum pump resulting in semi-solid organosilatanes (**6a–6c**).

2.2.1.1. Synthesis of (Z)-3-(2,8,9-trioxa-5aza-1sila-bicyclo[3.3.3]undecan-1yl)-N-(4-(prop-2-ynyloxy) benzylidene)propan-1amine (6a). The quantities used were as: **5** (0.10 g, 0.43 mmol), **2a** (0.07 g, 0.43 mmol). Yellow semi-solid, Yield: 96%. 1H NMR (500 MHz, Chloroform-*d*) δ : 8.15 (s, 1H, CH = N), 7.64 (d, J = 8.5 Hz, 2H, Ar-H), 6.94 (d, J = 8.8 Hz, 2H, Ar-H), 4.69 (d, J = 2.5 Hz, 2H, $-OCH_2$), 3.72 (t, J = 5.8 Hz, 6H, NCH_2CH_2OSi), 3.55 (t, J = 7.2 Hz, 2H, CH = NCH_2), 2.76 (t, J = 5.8 Hz, 6H, NCH_2CH_2OSi), 2.52 (t, J = 2.4 Hz, 1H, $C\equiv C-H$), 1.78–1.74 (p, J = 7.5 Hz, 2H, $-CCH_2C-$), 0.40 (t, J = 8.5 Hz, 2H, $-SiCH_2-$). ^{13}C NMR (126 MHz, Chloroform-*d*) δ : 159.60–159.11 (CH = N), 130.46–114.77 (Ar-C),

78.29 ($C\equiv C-H$), 75.77 ($C\equiv C-H$), 65.13 (CH = NCH_2), 59.57–57.02 (NCH_2CH_2OSi), 55.82 (OCH_2), 51.11 (NCH_2CH_2OSi), 26.59 (CCH_2C), 13.81 ($SiCH_2$). ESI-TOF-MS (m/z) Calcd. for $C_{19}H_{26}N_2O_4Si$: 375.51 [M + H], Found 375.18.

2.2.1.2. Synthesis of (Z)-3-(2,8,9-trioxa-5aza-1sila-bicyclo[3.3.3]undecan-1yl)-N-(3-methoxy-4-(prop-2-ynyloxy) benzylidene)propan-1amine (6b). The quantities used were as: **5** (0.10 g, 0.43 mmol), **2b** (0.08 g, 0.43 mmol). Yellow semi-solid, Yield: 92%. 1H NMR (500 MHz, Chloroform-*d*) δ : 8.13 (s, 1H, CH = N), 7.41–6.99 (m, 3H, Ar-H), 4.76 (d, J = 2.4 Hz, 2H, OCH_2), 3.89 (s, 3H, OCH_3), 3.73 (d, J = 5.8 Hz, 6H, NCH_2CH_2OSi), 3.57–3.53 (t, J = 7.2 Hz, 2H, CH = NCH_2), 2.76 (t, J = 5.8 Hz, 6H, NCH_2CH_2OSi), 2.50 (t, J = 2.4 Hz, 1H, $C\equiv C-H$), 1.78–1.75 (p, J = 7.5 Hz, 2H, $-CCH_2C-$), 0.41 (t, J = 8.6 Hz, 2H, $-SiCH_2-$). ^{13}C NMR (126 MHz, Chloroform-*d*) δ : 159.85 (CH = N), 149.78–109.32 (Ar-C), 78.27 ($C\equiv C-H$), 76.16–76.04 ($C\equiv C-H$), 65.09 (CH = NCH_2), 57.78 (OCH_3), 56.64–56.04 (NCH_2CH_2OSi), 55.95 (OCH_2), 51.09 (NCH_2CH_2OSi), 26.58–21.44 (CCH_2C), 13.82 ($SiCH_2$). ESI-TOF-MS (m/z) Calcd. for $C_{20}H_{28}N_2O_5Si$: 405.53 [M + H], Found 405.18.

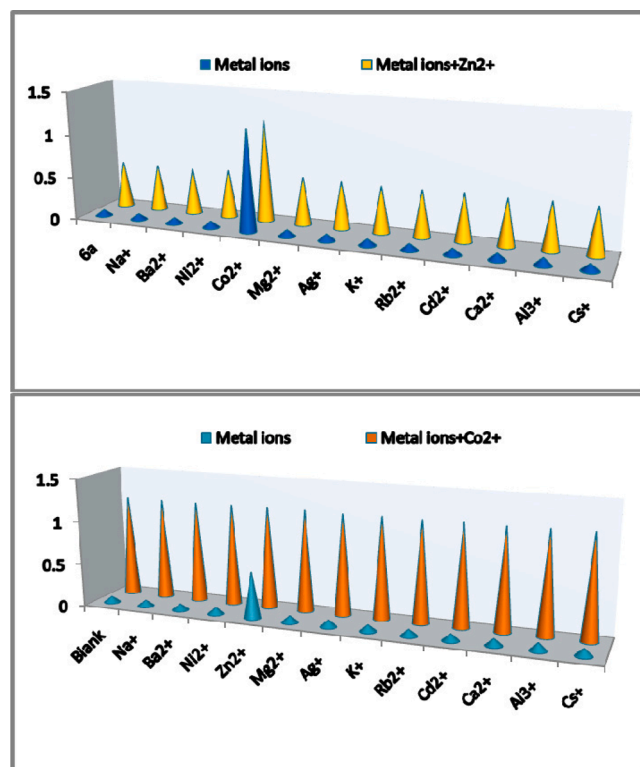


Fig. 3. Bar graph representation of interference study of compounds 6a in the presence of different competitive metal ions.

2.2.1.3. Synthesis of (Z)-3-(2,8,9-trioxa-5aza-1sila-bicyclo[3.3.3]undecan-1yl)-N-(3-ethoxy-4-(prop-2-ynyloxy) benzylidene)propan-1amine (6c). The quantities used were as: **5** (0.10 g, 0.43 mmol), **2c** (0.09 g, 0.43 mmol). Yellow semi-solid, Yield: 91%. ^1H NMR (500 MHz, Chloroform-*d*) δ : 8.12 (s, 1H, CH = N), 7.39–7.01 (m, 3H, Ar-H), 4.76 (d, J = 2.4 Hz, 2H, OCH₂), 4.12 (q, J = 7.0 Hz, 2H, OCH₂CH₃), 3.73 (t, J = 5.8 Hz, 6H, NCH₂CH₂OSi), 3.54 (t, J = 7.2 Hz, 2H, CH = NCH₂), 2.76 (t, J = 5.8 Hz, 6H, NCH₂CH₂OSi), 2.49 (t, J = 2.4 Hz, 1H, C \equiv C-H), 1.79–1.73 (m, 2H, -CCH₂C-), 1.43 (t, J = 7.0 Hz, 3H, OCH₂CH₃), 0.39 (t, J = 8.3 Hz, 2H, -SiCH₂-). ^{13}C NMR (126 MHz, Chloroform-*d*) δ : 159.91 (CH = N), 149.28–110.85 (Ar-C), 78.53 (C \equiv C-H), 75.93 (C \equiv C-H), 65.13 (CH = NCH₂), 64.42 (OCH₂CH₃), 59.52–56.95 (NCH₂CH₂OSi), 56.84 (OCH₂), 51.13 (NCH₂CH₂OSi), 26.60 (CCH₂C), 14.81 (CH₃), 13.83 (SiCH₂). ESI-TOF-MS (m/z) Calcd. for C₂₁H₃₀N₂O₅Si: 419.56 [M + H], Found 419.20.

2.2.1.4. Synthesis of (Z)-3-(2,8,9-trioxa-5aza-1sila-bicyclo[3.3.3]undecan-1yl)-N-(2-(prop-2-ynyloxy) benzylidene)propan-1amine (6d). The quantities used were as: **5** (0.10 g, 0.43 mmol), **2d** (0.07 g, 0.43 mmol). Brown semi-solid, Yield: 86%. ^1H NMR (500 MHz, Chloroform-*d*) δ : 8.64 (s, 1H, CH = N), 7.93–6.97 (m, 4H, Ar-H), 4.71 (d, J = 2.4 Hz, 2H, OCH₂), 3.71 (t, J = 5.8 Hz, 6H, NCH₂CH₂OSi), 2.74 (t, J = 5.8 Hz, 6H, NCH₂CH₂OSi), 2.55 (t, J = 4.5 Hz, 2H, CH = NCH₂), 2.52 (t, J = 2.4 Hz, 1H, C \equiv C-H), 1.80–1.73 (m, 2H, -CCH₂C-), 0.41 (t, J = 8.3 Hz, 2H, -SiCH₂-). ^{13}C NMR (126 MHz, Chloroform-*d*) δ : 156.67–156.10 (CH = N), 131.13–112.76 (Ar-C), 78.44 (C \equiv C-H), 75.33 (C \equiv C-H), 65.57 (CH = NCH₂), 59.37–57.00 (NCH₂CH₂OSi), 56.39 (OCH₂), 51.07 (NCH₂CH₂OSi), 26.68 (CCH₂C), 13.86 (SiCH₂). ESI-TOF-MS (m/z) Calcd. for C₁₉H₂₆N₂O₄Si: 375.51 [M + H], Found 375.17.

2.2.1.5. Synthesis of (Z)-3-(2,8,9-trioxa-5aza-1sila-bicyclo[3.3.3]undecan-1yl)-N-(3-methoxy-2-(prop-2-ynyloxy) benzylidene)propan-1amine (6e). The quantities used were as: **5** (0.10 g, 0.43 mmol), **2e** (0.08 g, 0.43 mmol). Pale yellow semi-solid, Yield: 87%. ^1H NMR (500 MHz, Chloroform-*d*) δ : 8.68 (s, 1H, CH = N), 7.56–6.89 (m, 3H, Ar-H), 4.72 (d, J = 2.4 Hz, 2H, OCH₂), 3.83 (s, 3H, OCH₃), 3.71 (t, J = 5.8 Hz, 6H, NCH₂CH₂OSi), 2.74 (t, J = 5.8 Hz, 6H, NCH₂CH₂OSi), 2.57 (t, J = 4.5 Hz, 2H, CH = NCH₂), 2.53 (t, J = 2.4 Hz, 1H, C \equiv C-H), 1.80–1.73 (m, 2H, -CCH₂C-), 0.40 (t, J = 8.3 Hz, 2H, -SiCH₂-). ^{13}C NMR (126 MHz, Chloroform-*d*) δ : 156.93 (CH = N), 152.53–113.62 (Ar-C), 78.99 (C \equiv C-H), 76.29 (C \equiv C-H), 65.45 (CH = NCH₂), 60.54–57.78 (NCH₂CH₂OSi), 55.82 (OCH₂), 51.10 (NCH₂CH₂OSi), 26.56 (CCH₂C), 13.92 (SiCH₂). ESI-TOF-MS (m/z) Calcd. for C₂₀H₂₈N₂O₅Si: 405.53 [M + H], Found 405.18.

2.3. Synthesis of 6a + Zn²⁺/Co²⁺ complex

The equimolar amount of organosilatrane **6a** and zinc chloride/cobalt chloride was added into the round bottom flask comprising 20 mL dry acetonitrile and then stirred for 4 h at 25 °C. The solvent was then removed under vacuum, which provides the yellow-colored precipitate.

3. Results and discussion

3.1. Synthetic aspects and characterizations

The route utilized for the synthesis of acetylene functionalized organosilatrane (**6a–6e**) is shown in Scheme 1. In the first step, the terminal alkynes (**2a–2e**) were prepared by reacting the substituted benzaldehyde with propargyl bromide in the presence of DMF solvent and potassium carbonate base. The second step includes the synthesis of γ -aminopropylorganosilatrane (**5**) by transesterification reaction between aminopropyltrimethoxysilane and triethanolamine by using dry toluene as a solvent and potassium hydroxide pellet as a catalyst. In this step, a dean stark apparatus was employed for the azeotropically removal of methanol and byproducts. In the final step, the alkynes (**2a–2e**) and γ -aminopropylorganosilatrane (**5**) were refluxed in dry toluene which results into the joining of these two compounds through Schiff-base linkage and formation of desired products (**6a–6e**). The para derivatives gave the higher yield (>90%) as compared to the ortho derivatives and among the para derivatives the **6a** was obtained with highest yield (96%). In ^1H NMR spectra, the triplet at 3.71–3.73 (NCH₂CH₂OSi), 2.74–2.76 (NCH₂CH₂OSi) and 0.39–0.41 (SiCH₂) confirm the formation of organosilatrane. The sharp singlet in the range of 8.15–8.68 and 2.49–2.53 confirms the presence of Schiff base protons (HC = N) and alkyne protons (C \equiv C-H) respectively. The methoxy protons showed a triplet around 3.83–3.89 while the ethoxy protons showed triplet and quartet at 1.43 and 4.12 respectively. In the ^{13}C NMR of all the organosilatrane (**6a–6e**), the highly deshielded imine carbon appeared in the region of 156.10–159.91 while the highly shielded methylene carbon (SiCH₂) appeared around 13.81. The carbons of the organosilatrane cage appeared in the range of 51.07–59.92. In the mass spectra, the base peak for all the compounds received at [M + H]. The obtained NMR (^1H and ^{13}C) and mass spectra match well with the structure of synthesized organosilatrane (**6a–6e**).

3.2. UV-visible study

UV-visible spectroscopy was employed to examine the photophysical properties of the compound **6a** in the absence and presence of various metal ions (Na⁺, Co²⁺, Ba²⁺, Ni²⁺, Zn²⁺, Mg²⁺, Ag⁺, K⁺, Rb²⁺, Cd²⁺, Ca²⁺, Al³⁺, Cs⁺). Firstly, the solution of **6a** (10⁻⁶ M) and metal

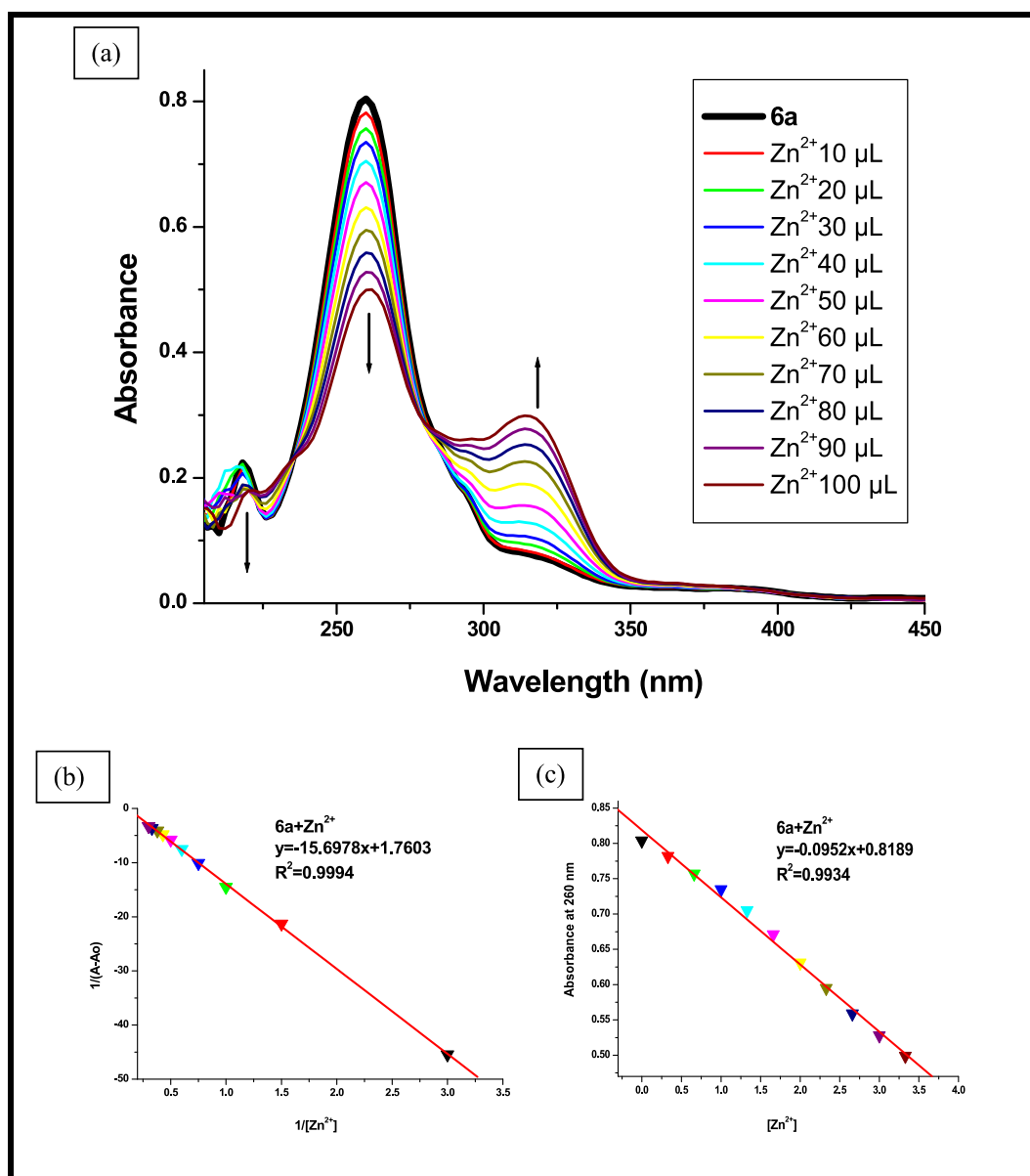


Fig. 4. UV-visible study of compound 6a (a) titration profile with varying concentration of Zn²⁺ ions from 10 to 100 µL (b) BH-plot at λ = 260 nm (c) linear calibration curve.

ions (10⁻² M) were prepared in acetonitrile and sufficient time was given for their complete mixing. After that, 10 µL of each metal solution was added one by one with the help of micropipette into the 3 mL of 10⁻⁶ M 6a solution taken into quartz cuvette and their respective UV-visible spectra were recorded. The 6a spectra alone showed three absorption bands at 218 nm, 260 nm and 312 nm due to π-π* electronic transitions. The spectra showed significant changes only in the presence of Zn²⁺ and Co²⁺ ions while the other metal ions did not bring any notable change in the spectra (Fig. 1). The selective recognition of Zn²⁺ and Co²⁺ ions may be due to the size of the cavity generated by silatrane 6a is similar to the size of these ions and both the ions fit into this cavity. A visible color change in the solution of 6a was also noticed in the presence of Co²⁺ ions (Fig. 2) and this change was also supported by the appearance of a band at 462 nm, which lies in the visible region.

To test the sensitivity of 6a towards Zn²⁺ and Co²⁺ ions, an

interference experiment was performed. In this experiment, we sequentially added the 100 µL of each competitive metal ion solution into the solution of 6a (3 mL) and Zn²⁺/Co²⁺ ions (10 µL) and recorded their UV-visible responses. Careful investigation of the spectra at λ = 312 nm showed no significant interference by the presence of other metal ions indicating the highly sensitive nature of 6a towards the identification of Zn²⁺ and Co²⁺ ions (Fig. 3).

For the UV-visible titration experiment, we dilute the solution of Zn²⁺ and Co²⁺ ions up to 10⁻⁴ M and then 10–100 µL was added into the 6a solution. After each successive addition, the spectra were recorded. The successive addition of both these metal ions displays

hypochromic shift at 260 nm and hyperchromic shift at 312 nm, but at 218 nm, the addition of Zn²⁺ ions exhibits the hypochromic shift while the addition of Co²⁺ ions exhibits hyperchromic shift (Figs. 4(a) and 5(a)). Also, no visible color change was noticed at this

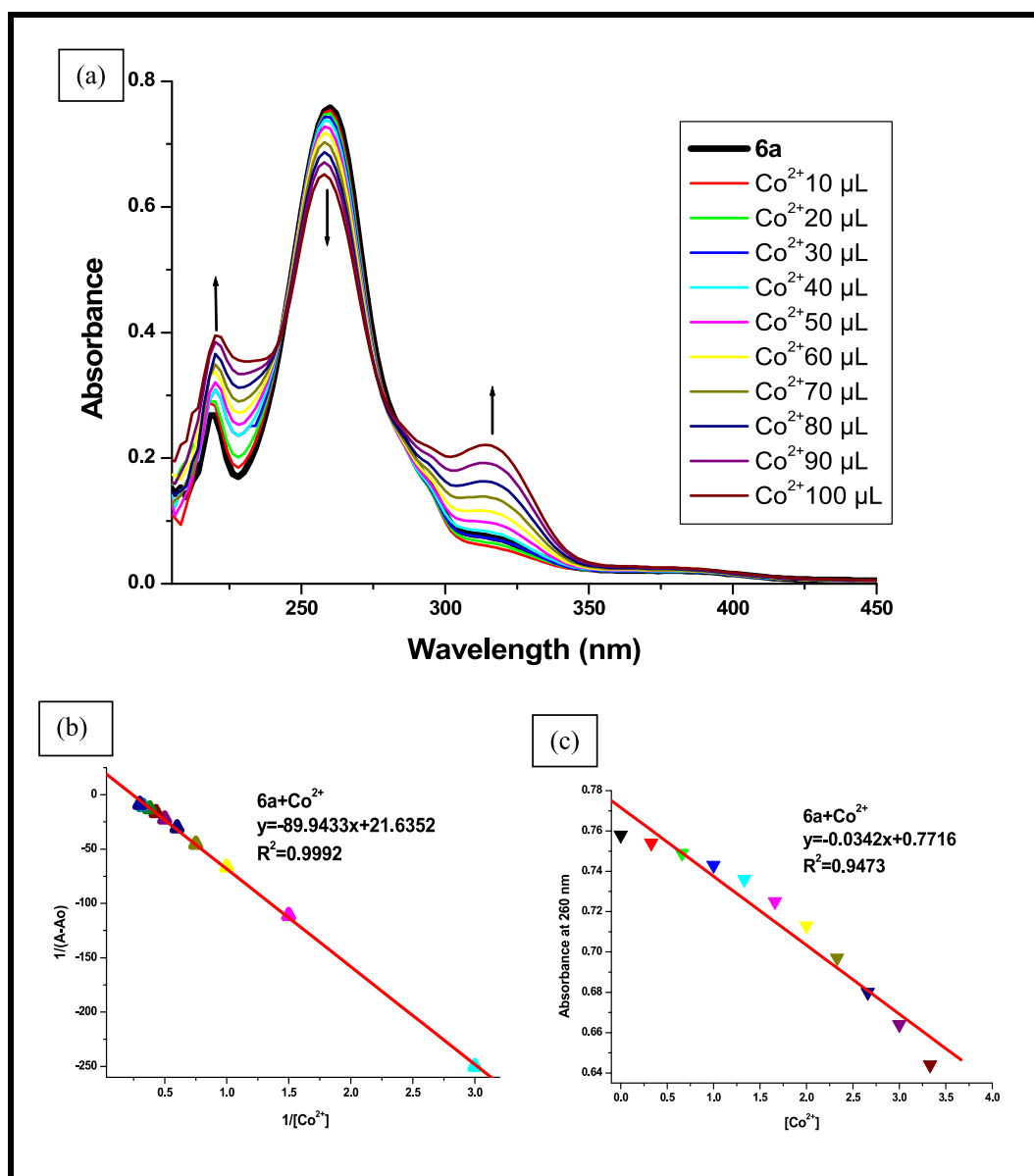


Fig. 5. UV-visible study of compound **6a** (a) titration profile with varying concentration of Co^{2+} ions from 10 to 100 μL (b) BH-plot at $\lambda = 260$ nm (c) linear calibration curve.

concentration.

Further, the stoichiometry and binding ability of **6a** with Zn^{2+} and Co^{2+} ions were examined by using the Benesi and Hildebrand (B-H) graphical method. In this methodology, by assuming 1: n stoichiometry between compound **6a** and metal ions, the equilibrium is expressed by the following Eq. (1).



$$\text{Association constant, } K_a = \frac{[\text{Analyte} \cdot \mathbf{M}^{2+}]_n}{[\text{Analyte}][\mathbf{M}^{2+}]^n} \quad (\mathbf{M} = \text{Co}^{2+}, \text{Zn}^{2+})$$

A graph is plotted between $[\text{A}-\text{A}_0]^{-1}$ vs. $[\text{Zn}^{2+}]^n$ and $[\text{Co}^{2+}]^n$ by using the UV-visible titration data at $\lambda = 260$ nm (Figs. 4(b) and 5(b)). Here $[\text{A}-\text{A}_0]$ denotes the change in absorbance intensity of compound **6a** upon the addition of metal ions. These graphs come out to be linear with

a high correlation coefficient value ($R^2 > 0.99$), which concludes that 1:1 stoichiometry of the complex. The association constant, $K_a = \text{intercept/slope}$ value for Zn^{2+} and Co^{2+} ions were $0.11 \times 10^6 \text{ M}^{-1}$ and $0.24 \times 10^6 \text{ M}^{-1}$ respectively which indicates the binding strength of **6a** towards Co^{2+} ions was almost double as compared to Zn^{2+} ions. Furthermore, the limit of detection, $\text{LOD} = 3 \times \text{standard deviation/slope}$ was calculated by plotting the linear calibration curves (Figs. 4(c) and 5(c)). The LOD values obtained for **6a** towards Zn^{2+} and Co^{2+} ions were $0.28 \times 10^{-6} \text{ M}$ and $0.82 \times 10^{-6} \text{ M}$ respectively which is less than the permissible value of Zn^{2+} (70 μM) and Co^{2+} (1.7 μM) ions in drinking water allowed by WHO (World Health Organisation) and EPA (Environmental Protection Agency) [6,13]. Table 1 shows that the synthesized organosilatrane **6a** is a better chemsensor for the detection of Zn^{2+} and Co^{2+} ions in comparison to the previously reported sensors because of its high association constant and low detection limit value.

Table 1

Comparative study of the analytical performance of newly synthesized sensor (**6a**) with the previously reported sensors.

Sensors	Metal ions	Ka (M ⁻¹)	LOD (M)	References
Thiophene-diocarbohydrazide derivative	Zn ²⁺	1.15 × 10 ⁴	0.15 × 10 ⁻⁶	6
Phenanthroline based sensor	Zn ²⁺	1.30 × 10 ⁶	0.84 × 10 ⁻⁶	9
Hexabodipy functionalized cyclotriphosphazenes	Co ²⁺	2.95 × 10 ⁶	0.84 × 10 ⁻⁶	12
Amide based sensor	Co ²⁺	8.90 × 10 ⁵	0.99 × 10 ⁻⁶	13
Quinoline and N', N'-dimethylethane-1,2-diamine based sensor	Zn ²⁺ Co ²⁺	1.30 × 10 ⁵ 4.0 × 10 ⁴	0.01 × 10 ⁻⁶ 6.89 × 10 ⁻⁶	15
Schiff base-acetylene functionalized organosilatrane	Zn ²⁺ Co ²⁺	0.11 × 10 ⁶ 0.24 × 10 ⁶	0.28 × 10 ⁻⁶ 0.82 × 10 ⁻⁶	Present work

3.3. Binding study by DFT and ¹H NMR

To understand the binding interactions between receptor **6a** and metal ions (Zn²⁺ and Co²⁺) theoretical DFT (Density Functional Theory) calculations were conducted on Gaussian 03 software. Firstly, the structure of **6a** was optimized in the absence and presence of Zn²⁺ and Co²⁺ ions by employing the B3LYP functional level and 6-31G(d) basis set for C, H, N, O atoms and LAN2DZ basis set for Zn²⁺ and Co²⁺ ions respectively (Fig. 6). Then highest occupied molecular orbit (HOMO) and lowest unoccupied molecular orbit (LUMO) was also created at the same level of theory and their respective energy values were noted (Fig. 7). Fig. 7 shows the electron density of HOMO and LUMO in **6a** and **6a-Zn²⁺**, mainly delocalized over Schiff-base, phenyl ring and slightly on propyl chain. In the case of **6a-Co²⁺** complex, singly occupied molecular orbitals (SOMO) and singly unoccupied molecular orbitals (SUMO) were produced as α-HOMO or β-HOMO and α-LUMO or β-LUMO rather than simple HOMO-LUMO according to their respective spin states. In **6a-Co²⁺** complex, the α, β-HOMO electron density was mainly distributed over silatranyl moiety and metal ions while the α, β-LUMO electron density was mainly distributed over metal ion, propyl

chain and somewhat on Schiff-base moiety. Hence, with the change in metal ions, there is a change in electronic distribution and molecular stability. It is noticed that the energy of both HOMO and LUMO decreases from **6a** to **6a-Zn²⁺/Co²⁺** system and the resulting decrease in energy gap (ΔE = E_{LUMO}-E_{HOMO}) from 0.1840 a.u. for **6a** to 0.1810 a.u. for **6a-Zn²⁺** ions, 0.0632 a.u. for the alpha of **6a-Co²⁺** ions and 0.0116 a.u. for the beta of **6a-Co²⁺** ions indicating the higher stability of the complex molecule. Further, the experimental evidence was taken into account by collecting the ¹H NMR of synthesized the **6a-Zn²⁺/Co²⁺** complex which showed a major shift in the organosilatrane protons from 3.72 ppm to 3.89 ppm (**6a-Zn²⁺**), 3.72 ppm to 3.65 ppm (**6a-Co²⁺**) and Schiff base protons from 8.15 ppm to 9.85 ppm, 8.15 ppm to 10.24 ppm indicating that the binding majorly occurs through these bonds (Fig. S16 and S17). Based on these, the proposed binding mechanism was shown in Scheme 2.

4. Conclusions

In this article, we have been successfully synthesized the acetylene functionalized organosilatrane (**6a-6e**) and well-characterized them with ¹H and ¹³C NMR spectroscopy and mass spectrometry. The UV-visible study of organosilatrane **6a** manifests their high selectivity and sensitivity towards the dual ion sensing of Zn²⁺ and Co²⁺ metal ions with detection limit 0.82 × 10⁻⁶ M and 0.28 × 10⁻⁶ M respectively. We expect that the synthesized chemosensor may offer opportunity for their applications in the field of industry and living sciences.

CRedit authorship contribution statement

Gurjaspreet Singh: Supervision, Project administration. **Sushma:** Conceptualization, Investigation. **Priyanka:** Methodology. **Suman:** Writing - original draft. **Diksha:** Writing - review & editing. **Jashan Deep Kaur:** Resources. **Anamika Saini:** Data curation. **Anita Devi:** Validation. **Pinky Satija:** Visualization.

Declaration of Competing Interest

The authors declare that they have no known competing financial interests or personal relationships that could have appeared to influence the work reported in this paper.

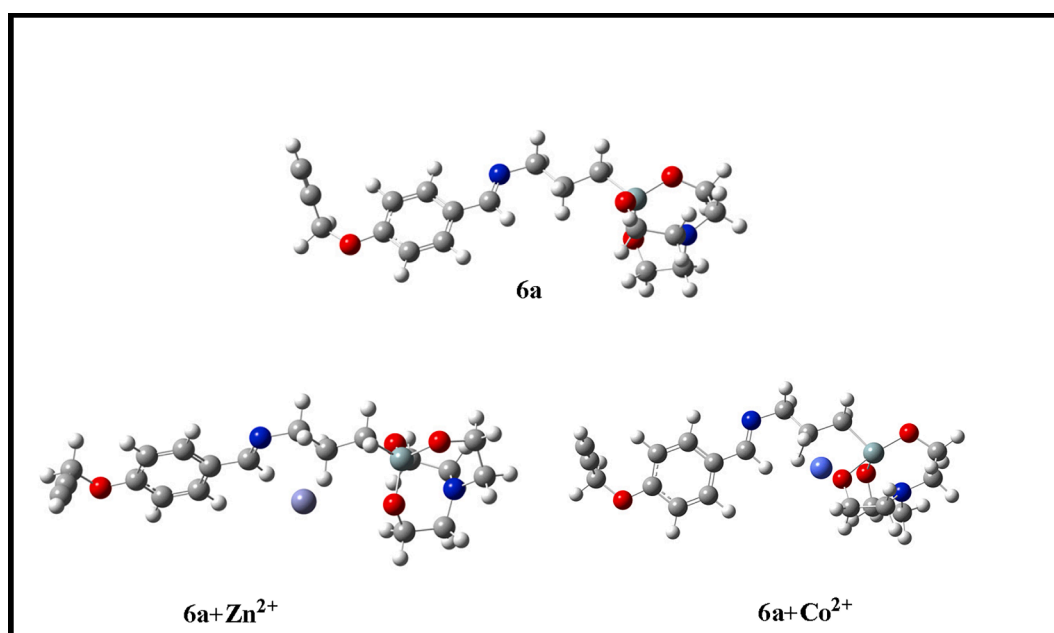


Fig. 6. Optimized structure of **6a** and its complex with Zn²⁺ and Co²⁺ ions.

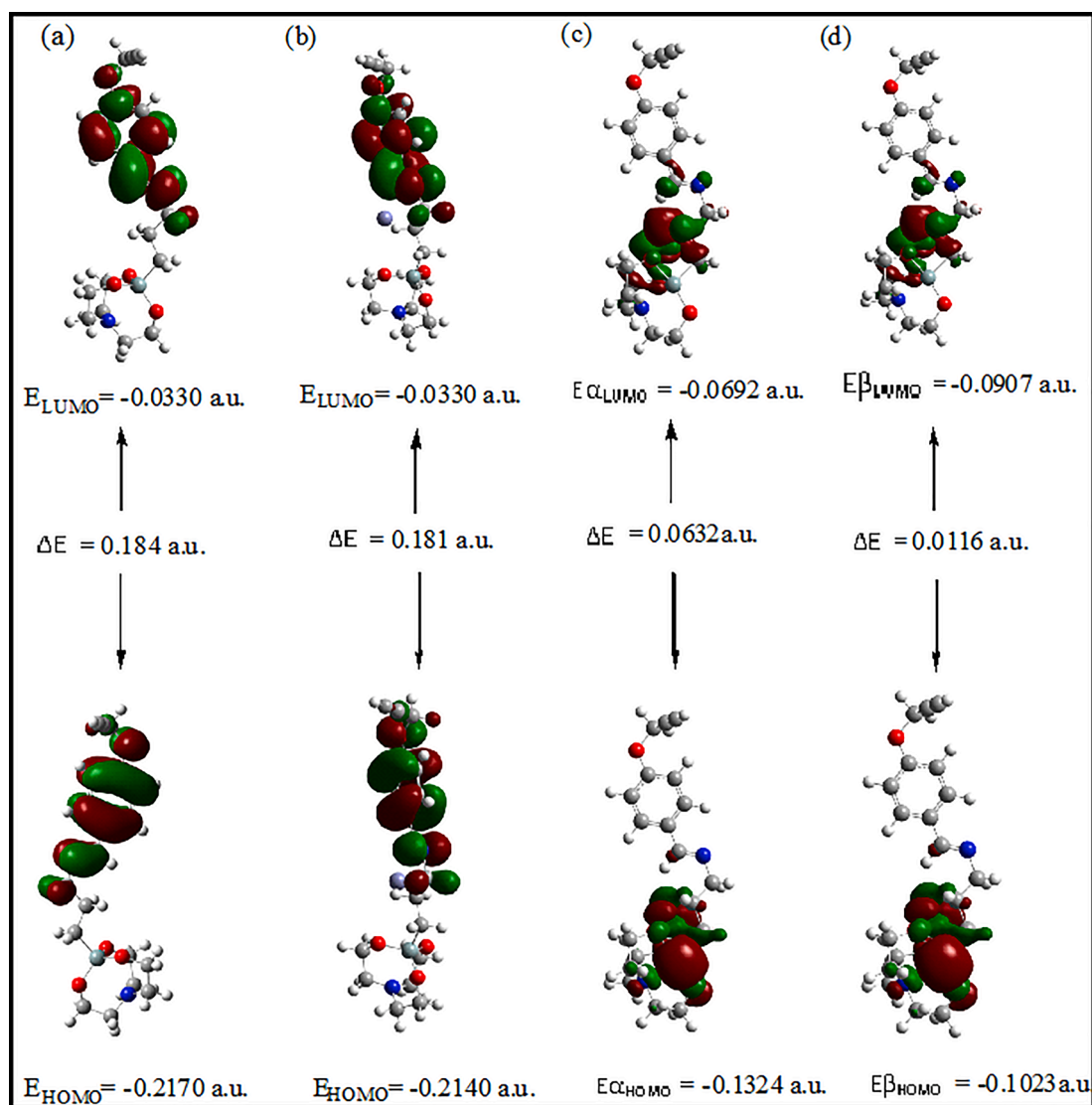
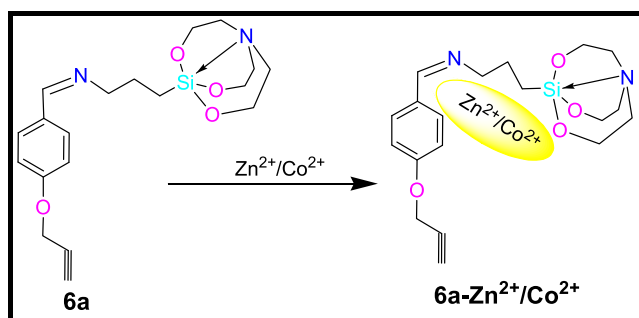


Fig. 7. DFT computed HOMO-LUMO diagram of (a) organosilatrane 6a, (b) 6a + Zn²⁺, (c) alpha MO of 6a + Co²⁺, (d) beta MO of 6a + Co²⁺.



Scheme 2. Possible mode of interactions between chemosensor 6a and metal ions Zn²⁺/Co²⁺.

Acknowledgements

The authors would like to thank UGC (MRP MA JOR-CHEM/2013/26532), DST PURSE II, DST SERB (SB/FT/CS-132/2014) and (CSIR (1 (2950)/18/EMR-11)), New Delhi for providing necessary financial support.

Appendix A. Supplementary data

Supplementary data to this article can be found online at <https://doi.org/10.1016/j.ica.2021.120465>.

References

- [1] A. Patil, S. Salunke-Gawali, Overview of the chemosensor ligands used for selective detection of anions and metal ions (Zn²⁺, Cu²⁺, Ni²⁺, Co²⁺, Fe²⁺, Hg²⁺), *Inorg. Chim. Acta* 482 (2018) 99–112, <https://doi.org/10.1016/j.ica.2018.05.026>.
- [2] R. Nagarajan, C. Varadaraju, K.H. Lee, Recent advancements in the role of *N*-Heterocyclic receptors on heavy metal ion sensing, *Dyes Pigm.* 191 (2021), 109331, <https://doi.org/10.1016/j.dyepig.2021.109331>.
- [3] D.T. Quang, J.S. Kim, Fluoro- and chromogenic chemodosimeters for heavy metal ion detection in solution and biospecimens, *Chem. Rev.* 110 (2010) 6280–6301, <https://doi.org/10.1021/cr100154p>.
- [4] X. Wang, G. Ding, Y. Duan, M. Wang, G. Zhu, X. Li, Y. Zhang, X. Qin, Novel 'naked-eye' Bis-Schiff base fluorescent chemosensors for sensitive detection of Zn²⁺ and bio-imaging in living cells, *Tetrahedron* 76 (2020), 131108, <https://doi.org/10.1016/j.tet.2020.131108>.
- [5] P. Banumathi, G. Tamil selvan, M. Selvakumar Paulraj, P. Rajasingh, Synthesis of antipyrine based organic material for Zn²⁺ ion sensing and implication in logic gate analysis, *Mater. Today Proc.* (2020), <https://doi.org/10.1016/j.matpr.2020.07.084>.
- [6] M. Mary Mathew, A. Sreekanth, Zn²⁺ ion responsive fluorescent chemosensor probe of Thiophene-dicarbohydrazone derivatives, *Inorg. Chim. Acta* (516 2021), 120149, <https://doi.org/10.1016/j.ica.2020.120149>.

- [7] H. He, Z. Cheng, L. Zheng, Aqueous Zn^{2+} analysis: Specific recognition and instant imaging by Schiff base fluorescent probes, *J. Mol. Struct.* 1227 (2021), 129522, <https://doi.org/10.1016/j.molstruc.2020.129522>.
- [8] Y.T. Huang, S.Y. Cai, X.L. Ruan, S.Y. Chen, G.F. Mei, G.H. Ruan, D.D. Cao, Salicylic acid enhances sunflower seed germination under Zn^{2+} stress via involvement in Zn^{2+} metabolic balance and phytohormone interactions, *Sci. Hortic. (Amsterdam)* 275 (2021), 109702, <https://doi.org/10.1016/j.scienta.2020.109702>.
- [9] Z. Aydin, A novel phenanthroline-based colorimetric turn-off optical sensor for Zn^{2+} , *Inorg. Chim. Acta* 517 (2020), 120200 <https://doi.org/10.1016/j.ica.2020.120200>.
- [10] S. Valet, A. Burkert, G. Ebell, M. Babutzka, Determination of the corrosion product layer resistance on zinc and electrolytically galvanized steel samples by using gel electrolytes, *Electrochim. Acta* 385 (2021), 138191, <https://doi.org/10.1016/j.electacta.2021.138191>.
- [11] X. Zhang, L. Wang, H. Fu, Recent advances in rechargeable Zn-based batteries, *J. Power Sources* 493 (2021), 229677, <https://doi.org/10.1016/j.jpowsour.2021.229677>.
- [12] E. Şenkuytu, E. Tanrıverdi Eşik, New hexa-bodipy functionalized dendrimeric cyclotriphosphazene conjugates as highly selective and sensitive fluorescent chemosensor for Co^{2+} ions, *Spectrochim. Acta A* 198 (2018) 232–238, <https://doi.org/10.1016/j.saa.2018.03.002>.
- [13] K.Y. Ryu, S.Y. Lee, D.Y. Park, S.Y. Kim, C. Kim, A novel colorimetric chemosensor for detection of Co^{2+} and S^{2-} in an aqueous environment, *Sens. Actuators B Chem.* 242 (2017) 792–800, <https://doi.org/10.1016/j.snb.2016.09.180>.
- [14] Y. Wu, Y. Liu, J. Yin, H. Li, J. Huang, Facile ultrasonic synthesized NH_2 -carbon quantum dots for ultrasensitive Co^{2+} ion detection and cell imaging, *Talanta* 205 (2019), 120121, <https://doi.org/10.1016/j.talanta.2019.120121>.
- [15] G. Jin, J. Jun, G. Rim, L. Nguyen, I. Noh, C. Kim, A dual chemosensor for Zn^{2+} and Co^{2+} in aqueous media and living cells: Experimental and theoretical studies, *Sens. Actuators B Chem.* 223 (2016) 509–519, <https://doi.org/10.1016/j.snb.2015.09.129>.
- [16] G. Singh, A. Priyanka, P.S. Singh, P. Sushma, J. Mohit, J.S. Singh, Schiff base-functionalized silatrane-based receptor as a potential chemo-sensor for the detection of Al^{3+} ions, *New J. Chem.* 45 (2021) 7850–7859, <https://doi.org/10.1039/d1nj00943e>.
- [17] P. Ilanchezhian, C. Siva, H.D. Cho, S. Tamilselvan, S. Seal, T.W. Kang, D.Y. Kim, Aid of cobalt ions in boosting the electrocatalytic oxygen and hydrogen evolution functions of $NdFeO_3$ perovskite nanostructures, *J. Mater. Res. Technol.* 11 (2021) 2246–2254, <https://doi.org/10.1016/j.jmrt.2021.02.047>.
- [18] Y. Feng, G. Ying, Z. Yang, K. Shih, H. Li, D. Wu, Chemosphere Sulfate radical-induced destruction of emerging contaminants using traces of cobalt ions as catalysts, *Chemosphere.* 256 (2020), 127061, <https://doi.org/10.1016/j.chemosphere.2020.127061>.
- [19] K. Shen, K. Sheng, Z. Wang, J. Zheng, C. Xu, Cobalt ions doped tungsten oxide nanowires achieved vertically aligned nanostructure with enhanced electrochromic properties, *Appl. Surf. Sci.* 501 (2020), 144003, <https://doi.org/10.1016/j.apsusc.2019.144003>.
- [20] G. Singh, S. Rani, A. Arora, H. Sanchita, D.M. Duggal, Organic-inorganic nano-hybrid decorated by copper (II) incarceration: A versatile catalytic assembly for the swift reduction of aromatic nitro and dye compounds, *Mol. Catal.* 431 (2017) 15–26, <https://doi.org/10.1016/j.mcat.2017.01.026>.
- [21] G. Singh, A. Arora, P. Kalra, I.K. Maurya, C.E. Ruiz, M.A. Estebanc, S. Sinha, K. Goyal, R. Sehgal, A strategic approach to the synthesis of ferrocene appended chalcone linked triazole allied organosilatrane: Antibacterial, antifungal, antiparasitic and antioxidant studies, *Bioorg. Med. Chem.* 27 (2019) 188–195, <https://doi.org/10.1016/j.bmc.2018.11.038>.
- [22] G. Singh, A. Sanchita, G. Singh, P. Sharma, P.S. Kalra, S. Diksha, V.V. Soni, Ester appended organosilatrane: Paradigm for the detection of Cu^{2+} , Pb^{2+} and Hg^{2+} ion, *Inorg. Chim. Acta* 490 (2019) 85–92, <https://doi.org/10.1016/j.ica.2019.03.008>.
- [23] W. Tanglumlert, P. Prasassarakich, P. Supaphol, S. Wongkasemjit, Hard-coating materials for poly(methyl methacrylate) from glycidoxypropyltrimethoxysilane-modified silatrane via a sol-gel process, *Surf. Coat. Technol.* 200 (2006) 2784–2790, <https://doi.org/10.1016/j.surfcoat.2004.11.018>.
- [24] A. Upadhyay, A.K. Purohit, G. Mahakur, S. Dash, P.K. Kar, Verification of corrosion inhibition of Mild steel by some 4-Aminoantipyrine-based Schiff bases - Impact of adsorbate substituent and cross-conjugation, *J. Mol. Liq.* 333 (2021), 115960, <https://doi.org/10.1016/j.molliq.2021.115960>.
- [25] B. Naureen, G.A. Miana, K. Shahid, M. Asghar, S. Tanveer, A. Sarwar, Iron (III) and zinc (II) monodentate Schiff base metal complexes: Synthesis, characterisation and biological activities, *J. Mol. Struct.* 1231 (2021), 129946, <https://doi.org/10.1016/j.molstruc.2021.129946>.
- [26] S. Swami, N. Sharma, A. Agarwala, V. Shrivastava, R. Shrivastava, Schiff base anchored silver nanomaterial: An efficient and selective nano probe for fluoride detection in an aqueous medium, *Mater. Today Proc.* (2021) 1–7, <https://doi.org/10.1016/j.matpr.2021.01.269>.
- [27] J. Singh, S. Thakur, R. Singh, V. Kaur, Schiff base - Zn^{2+} ion combo as 'pick and degrade' probe for selected organophosphorus chemical weapon mimics and flame retardant analog: Detoxification of fruits and vegetables in aqueous media, *Food Chem.* 327 (2020), 127080, <https://doi.org/10.1016/j.foodchem.2020.127080>.
- [28] G. Singh, A.S. Pawan, D. Shilpy, G. Suman, S.C. Sharma, A.K. Sahoo, Propargyl-functionalized single arm allied Anthracene based Schiff bases: Crystal structure, solvatochromism and selective recognition of Fe^{3+} ion, *J. Mol. Struct.* 1229 (2021), 129618, <https://doi.org/10.1016/j.molstruc.2020.129618>.
- [29] G. Singh, P. Kalra, A. Arora, A. Singh, G. Sharma, Sanchita, I.K. Maurya, S. Dutta, P. Munshi, V. Verma, Acetylenic Indole-Encapsulated Schiff Bases: Synthesis, In Silico Studies as Potent Antimicrobial Agents, Cytotoxic Evaluation and Synergistic Effects, *ChemistrySelect*, 3 (2018) 2366–2375. <https://doi.org/10.1002/slct.201703018>.
- [30] G. Singh, A. Sushma, P.S. Singh, M. Shilpy, J. Priyanka, A.K. Singh, Schiff base derived bis-organosilanes: Immobilization on silica nanosphere and Cu^{2+} and Fe^{3+} dual ion sensing, *Inorg. Chim. Acta* 514 (2021), 120028, <https://doi.org/10.1016/j.ica.2020.120028>.



Dr. Gurjaspreet Singh is a Professor in the Department of Chemistry at Panjab University, Chandigarh, India. He has more than 22 years of experience in teaching as well as in research. He is highly expertise in Organometallics, Bio-Inorganic, Organotransition chemistry. His research work is primarily based on the Chemistry of Organosilicon compounds focusing precisely on the design, synthesis, characterization and properties of new organic compounds especially the biological activity of bonded metals. He had published more than 100 research papers in various internationally peer reviewed journals. He had the privilege in introducing Click Silylation term in Organosilicon chemistry and using this term he has published more than 30 papers in internationally peer reviewed journals. Till date, 21 students had completed their doctorate degree under his supervision. Apart from Ph.D students, till date, he had also acted as a supervisor of the M.Sc students (more than 80) for their dissertation work. He had successfully completed UGC, DST SERB and CSIR major research projects with 80 publications. A lot of his research work has been presented in various conferences and in professional meetings. He is a Life member of Chemical Research Society of India and of the Indian Science Congress Association. He has been reviewing the research articles for the various international peer reviewed journals.